Inorganica Chimica Acta 492 (2019) 131–141

Contents lists available at ScienceDirect

Inorganica Chimica Acta

journal homepage: www.elsevier.com/locate/ica

Research paper

Synthesis and characterisations of copper(II) complexes of 5-methoxyisatin thiosemicarbazones: Effect of N-terminal substitution on DNA/protein binding and biological activities

K.N. Aneesrahman[a], K. Ramaiah[b], G. Rohini[a], G.P. Stefy[a], N.S.P. Bhuvanesh[c], A. Sreekanth[a,*]

[a] Department of Chemistry, National Institute of Technology, Tiruchirappalli 620015, India
[b] Department of Chemistry, National Institute of Technology, Warangal 506004, India
[c] Department of Chemistry, Texas A & M University, College Station, TX 77842, USA

ARTICLE INFO

Keywords:
Isatin derivatives
Copper(II) complexes
DNA/BSA interaction
Antimicrobial
Antioxidant
In vitro anti-proliferative activity

ABSTRACT

The newly synthesized ligands (**HL1**-**HL3**) of 5-methoxyisatin thiosemicarbazone with different N-terminal substituents and their copper(II) complexes **1–3** respectively were exposed to spectral and structural characterization. The spectral studies reveal that the ligands show a tridentate mode of binding (ONS donor) with Cu (II) to form square planar complexes. The crystal structure of the ligand **HL1** and complex **1** were confirmed by single crystal XRD. The compounds were subjected to DNA/BSA interaction studies using electronic and fluorescence spectroscopic techniques. The binding studies showed that, the complexes (**1–3**) were able to bind with DNA/BSA macromolecules with good binding constant. In which **1** ($K_b = 0.83 \times 10^5\,M^{-1}$) shows good interaction with the DNA while **3** shows better interaction with BSA ($K_b = 2.4 \times 10^5\,M^{-1}$). The complexes (**1–3**) were also tested for antimicrobial activity, radical scavenging activity and *in vitro* anti-proliferative activity. Complex **3** have shown potent efficacy with broad spectrum antimicrobial activity against the microorganisms, whereas the complex **1** has shown decent scavenging properties compared to the reference drug (ascorbic acid) with an IC_{50} value of 19.23 ± 1.05 μM. Further the, anti-proliferative activity study revealed that, the complex **1** has exhibited broad spectrum activity against MCF-7, A549 and HeLa with IC_{50} values 14.83 ± 0.45 μM, 17.88 ± 0.16 μM and 6.89 ± 0.42 μM, respectively compared to standard drug Doxorubicin.

1. Introduction

Cisplatin being a successful model in the medical treatment of several types of tumours, has made greater interest in developing metal-based drugs. Even though the cisplatin is effective in healing varieties of cancers, their limitations such as resistance, serious toxicity and other side effects [1] forces the chemists to search for alternative metallo-drugs with more efficient, target specific and less toxicity. As a result, numerous metal complexes with deferent combinations of metals and ligands were reported [2].

The selection of metal ion is one of the significant factors in the development of metal-based therapeutic agent. The copper compounds have been active in research since 1980s. Copper is known to be bio-essential metal in the human body and is a catalytic and structural centre of many metalloenzymes and proteins. Hence copper involved in many redox active mechanisms such as antioxidative activity (SOD) and energy metabolism [3]. Therefore biologically compatible copper(II) complexes are one of the better choices for the cellular level medicinal applications as therapeutic agents. There were copper(II) complexes of Schiff bases have been reported with good chemical nuclease activity [4,5], Moreover, a number of copper complexes have been reported as potential antitumor substances, proving significant anticancer activity while maintaining lower toxicity than cisplatin [6–8].

The earlier studies on platinum complexes showed the significance of the ligands in tuning the activity and efficiency of metal complexes [9,10]. Hence the choice of ligand is also important in the metal complex based drugs. Literature shows that thiosemicarbazones (TSC) are the class of ligands with remarkable biological activity and medicinal properties [11–13]. TSCs shows wide spectrum of biological activities such as antitumour [14], antiviral [15], anti-HIV [16], anti-fungal [17,18], antimalarial [19], antibacterial [20], anti-filarial activities [21]. The biological activities of the TSCs can improve significantly by complex formation with various metal ions. The thiosemicarbazone complexes of transition metals with the successful

* Corresponding author.
E-mail address: sreekanth@nitt.edu (A. Sreekanth).

https://doi.org/10.1016/j.ica.2019.04.019
Received 8 November 2018; Received in revised form 1 March 2019; Accepted 10 April 2019
Available online 11 April 2019

demonstration of anticancer activities have been reported [22,23].

The present work discusses copper complexes of 5-methoxyisatin 4N-substituted thiosemicarbazones ligands. Previous reports are suggesting that, 4N-substitution can alter the activities of the thiosemicarbazones and its complexes [24–26]. Thiosemicarbazones are usually less soluble water, which may reduce its bioavailability at the same time, the hydrophobicity or lipophilic nature is an important factor for a molecule its cell availability. Hence the right balance between a molecule's hydrophilicity, which promotes solubility and bioavailability, and lipophilicity, which allows these molecules for the cell membrane permeability through lipidic bilayer, is an essential requirement for an efficient drugs and its cellular uptake [27]. Three different terminal substituent have chosen for the present study, they are pyrrolidine, morpholine and cyclohexyl ammine. When these molecules are fused into the TSCs, and considering the polar nature and hydrogen bonding capability with the water molecules, pyrrolidine substituent become more hydrophobic and cyclohexyl substituted TSC become less hydrophobic due to the presence hydrogen at 4 N position and possible hydrogen bonding interactions. On this basis, the study also aim to look the influence various fragments on the terminal amino group on various biological studies. The synthesised compounds were explored for their *in vitro* antibacterial, antifungal, scavenging and antiproliferative studies along with DNA and Protein binding studies.

2. Results and discussion

2.1. Synthesis

The Schemes 1 and 2 represent the synthesis of ligands (**HL1**-**HL3**) and their copper(II) complexes (**1**–**3**). Both the ligands and complexes are air stable and non-hydrophobic. All the ligands (orange to orange red) and complexes (chocolate) coloured powder. Both ligands and complexes are insoluble in water and common organic solvents but soluble in DMSO and DMF. The ligands are slightly soluble in methanol. Mass and elemental analysis of the complexes suggested that the ligand and metal ratio of the complex is 1:1 of the type [M(L)(Cl)]. Here the L indicates the deprotonated ligands. The structure of **HL1** and **1** was further elucidated by single crystal X-ray diffraction method.

2.2. Spectroscopy

Electronic absorption spectra (Figs. S1 and S2) of the ligands (**HL1**-**HL3**) exhibited significant bands around 286–305 nm and 348–381 nm, attributable to π–π^* and n–π^* transitions, respectively. Whereas, a slight shift in energy of these bands were observed on complexation. The spectra of the complexes (**1**–**3**) showed bands in the range 269–274 nm and 346–361 nm, corresponds to π–π^* and n–π^* intra ligand transitions. Additionally, a third band was observed for complexes in the range of 416–422 nm, as a result of the S → Cu(II) ligand to metal charge transfer (LMCT) transition, spreading in to the visible region [28]. The spectra of the complexes in solution did not show the absorption band responsible for the d–d transition. But the solid-state DRS spectra exhibited a d–d band as a weak shoulder band in the range of 610–640 nm [29–31].

In the FT-IR spectra, ligands showed bands in the range of 3376–3471, 3136–3281, 1691–1693, 1525–1593 and 1341–1349 cm^{-1}, which were ascribed to the stretching vibrations of indole N—H, azomethine N—H, C═O, C═N and C═S groups, respectively (Figs. S3–S5). Both N—H vibrations were showed weak bands for all ligands. In **HL3**, a weak band was observed at 3239 cm^{-1}, which was assigned to the terminal N—H. The intensities of carbonyl vibrations was medium for **HL1** while strong for **HL2** and **HL3**. Complexation causes the shifting of these bands considerably (Figs. S6–S8). There was a shift in the frequencies of carbonyl (1656–1663 cm^{-1}), and thiocarbonyl (1326–1332 cm^{-1}) groups. Intensities of both bands were reduced (strong to medium for υC═O and medium to weak for C═S). Furthermore, the band at 3136–3278 cm^{-1} was disappeared, which was due to the deprotonation of the azomethine N—H and resulted in the appearance of new bands in the region with medium to strong intensities at 1580–1628 cm^{-1} region, corresponding to the newly formed N═C due to the coordination *via* thiol sulfur [28,32,33]. The appearance of new bands in Far IR region of the spectra resultant to the metal-ligand vibrations further confirms the formation of the complexes (Figs. S9–S11). The υ(Cu—N) stretching frequencies for the azomethine nitrogen are observed around 278–280 cm^{-1} region. The formation of new band in the 260–263 cm^{-1} range was assigned to υ (Cu—S), is another evidence for the involvement of sulfur coordination from the ligands. All complexes showed strong υ(Cu—Cl) vibrations at 319–320 cm^{-1} region indicating the Cu—Cl bond in the complexes. The presence of new bands at 460–469 cm^{-1} range corresponding to the υ (Cu—O), proves the coordination of Oxygen from the carbonyl group of isatin to the copper center [28,34,35]. Thus, it suggested that the thiosemicarbazone coordinates to Cu(II) through an ONS donor atoms from thiosemicarbazone ligands.

The NMR spectra were recorded for the ligands (**HL1**-**HL3**) in DMSO-d_6 solvent and the detailed NMR data of each ligand are given in the experimental section. In the ^{1}H NMR spectra of the ligands, the H—N—C═S proton resonates at 12.72–13.38 ppm. The signals of pyrrolidine, morpholine and cyclohexyl protons on the terminal N of thiosemicarbazone appeared as multiplets in the region 4.01–1.09 ppm. The amide N—H proton is in the range of 10.84–11.15 ppm. All the aromatic protons are seen as multiplets around 6.87–7.09 ppm. The methoxy substituent in the ligands showed signal as a singlet peak in the range of 3.42–3.81 ppm. In **HL3** the thiosemicarbazone terminal N—H proton showed a singlet at 7.90 ppm. The ^{13}C NMR spectra of the ligands showed the chemical shift values at 175.8–179.9, 163.2–163.4, 155.7–155.8 ppm due to C═S, C═O and C═N groups, respectively. The aromatic carbon was observed in the range, 136.9–106.9 ppm. The

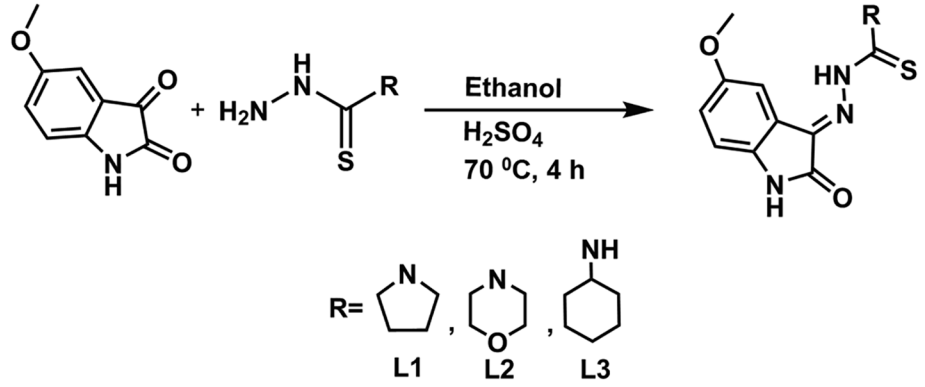

Scheme 1. Synthesis of 5-methoxyisatinthiosemicarbazone derivatives (**HL1**-**HL3**).

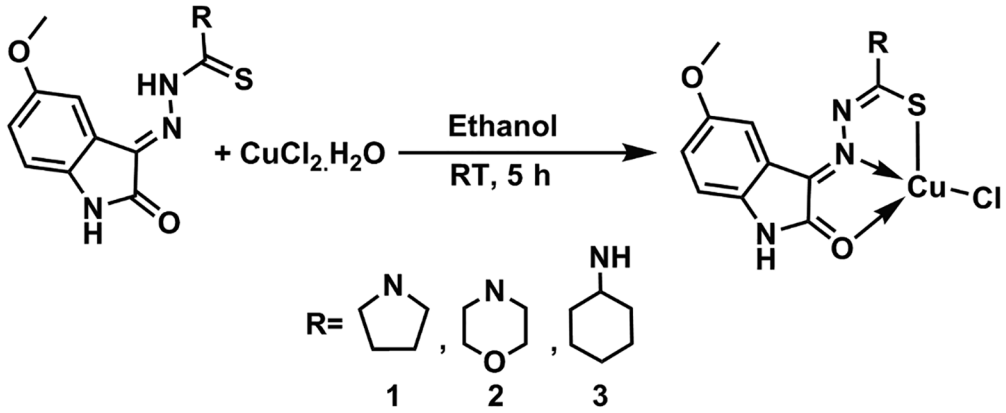

Scheme 2. Synthesis of copper(II) complexes (**1–3**).

peak corresponding to methoxy carbon was seen at 56.09 ppm, and the signals of the aliphatic carbon present on the terminal N of thiosemicarbazone appeared in the region of 66.19–24.12 ppm.

The ESR spectra of all the Cu(II) complexes were recorded in DMF solution at liquid nitrogen temperature (Figs. 1 and S12). The spectral data of all the complexes are given in Table 1. The ESR spectra of Cu(II) complexes show two peaks, one of small intensity towards low field region and the other of large intensity towards high field region. From these peaks the vales of $g_{\|}$ and $g_{\perp}$ have been calculated [36]. The g-values of Cu(II) complexes can be used to derive the ground state. In elongated octahedral and square planar complexes, the unpaired electron lies in the $d_{x^2-y^2}$ orbital giving $^2B_{1g}$ as the ground state with $g_{\|} > g_{\perp}$. In a compressed octahedron, on the other hand, the unpaired electron lies in d_{z^2} orbital giving $^2A_{1g}$ as ground state with $g_{\|} < g_{\perp}$. From the observed values (Table 1) it is evident that the unpaired electron lies predominantly in the $d_{x^2-y^2}$ orbital characteristic of square planar geometry [35]. Recalling the complexes with $d_{x^2-y^2}$ ground state, strong interaction along Z axis is to be accompanied by increase in the value of $g_{\|}$. Strong axial bonding leads to an increase in the length of the bond in the x-y plane which results in a decrease of both in plane covalency and the energy of $d_{x^2-y^2}$ transition. Both these effects tend to increase the value of $g_{\|}$. The $g_{\|}$is the most sensitive function for indicating the covalency, being 2.3 or more for ionic compounds and less than 2.3 for covalent compounds [37,38]. It is clear from Table 1 that $g_{\|}$ obtained is less than 2.3 indicating covalent character of the metal–ligand bond. The axial symmetry parameter G defined as $(g_{\|} - 2.0023)/(g_{\perp} - 2.0023)$ is shown to be a measure of the exchange interaction between copper centres in the polycrystalline solids. According to

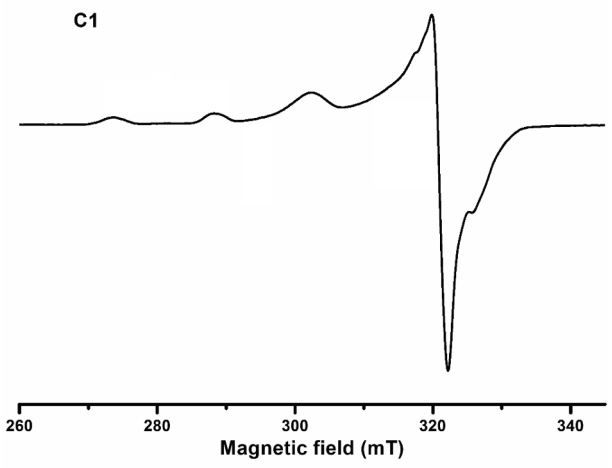

Fig. 1. X-band EPR spectrum of complex **1** in frozen DMF solution.

Table 1
EPR parameters of complexes **1–3**.

Complex	$g_{\|}$	$g_{\perp}$	G	$A_{\|}$(mT)
1	2.214	2.043	5.20	14.55
2	2.217	2.051	4.40	14.33
3	2.219	2.039	5.90	14.43

Hathaway and Billing [39], If the value of G is larger than 4, the exchange interaction is negligible while G values of less than 4 indicate considerable interaction in solid complexes. The present G values are found to be greater than 4, indicating that there is no exchange interaction in the solid state, further confirms the mononuclear nature of the complexes.

2.3. Single crystal X-ray crystallographic studies

The crystal structures of the ligand **HL1** and the complex **1** are shown in Fig. 2. The crystal data and structure refinement parameters, selected bond lengths and bond angles are listed in Tables 2, 3 and S1–S3). The **HL1** crystallized in the triclinic crystal system with space group $P-1$ with two molecules in the unit cell. The molecule is in thione form with trance configuration of the thiocarbonyl group and isatin moiety with respect to N2−N3 bond (Fig. 2b). The bonds in the −C═N−N═C(═S)−N skeleton of the molecules shows partial double bond and single bond character (Table 2) indicates the delocalization of π electrons over the −C═N−N═C(═S)−N chain. Structure of the compound brings out quasi-coplanarity of the whole molecular skeleton which was evidenced by torsional angles. The crystal structure further reveals an intramolecular hydrogen bonding between hydrazinic hydrogen (N3–H) and the oxygen of indole carbonyl (C1═O1). Further, there is an intramolecular hydrogen bonding between the hydrogen on the indole (N−H) and the water molecule in the crystal lattice (Table S2). The complex **1** was crystallised in a monoclinic crystal system with a space group of *P1211* and consists of two separate mononuclear Cu(II) complexes in the unit cell (Fig. 2b). The Cu(II) centre is in a (4 + 1) square-pyramidal coordination geometry, in which the thiosemicarbazone ligand (**HL1**) is coordinated in a tridentate manner through oxygen (O1), nitrogen (N1) and sulphur (S1). The fourth coordination is occupied by chloride ion, forming an equatorial plane of square-pyramidal geometry. The DMSO molecule in the lattice is coordinated to the copper centre *via an* oxygen atom (O3) at the axial position. In the equatorial plane, the two angles S1−Cu1−O1 and N1−Cu1−Cl1 between the trans-oriented ligator atoms are 162.68(17)° and 164.6(2)°, respectively. Furthermore, the summation of the angles (Table 3) between the donor atoms around the Cu1 is 357° (360° ideal value for in-plane angles), affirming distortion from perfect square planar geometry [40]. The azomethane N−H proton of **HL1** was deprotonated during the

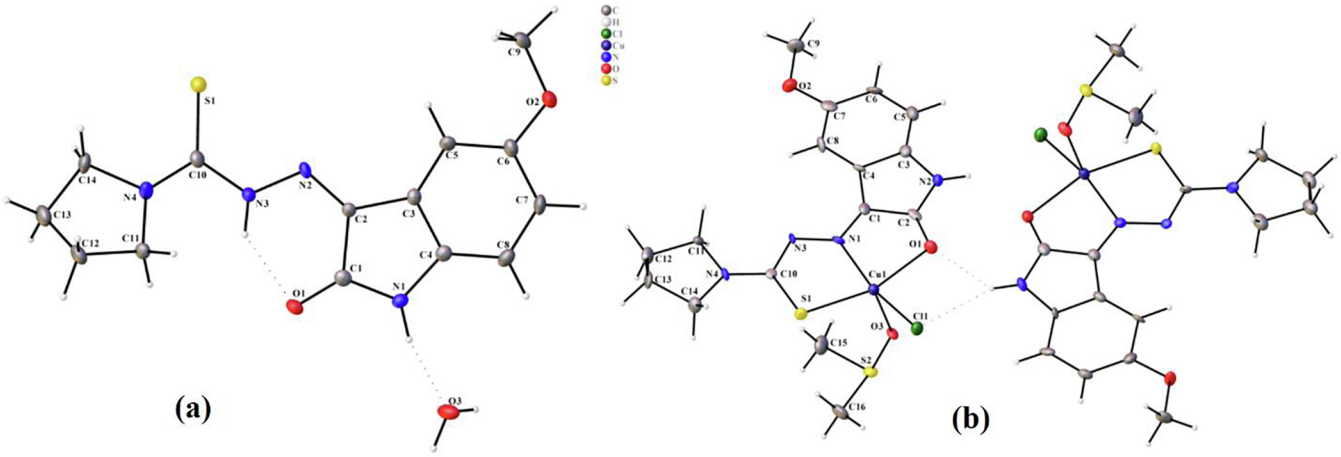

Fig. 2. (a) Thermal ellipsoid plot of **HL1** and (b) Thermal ellipsoid plot of **1**.

Table 2
Selected bond lengths (Å), angles (°) of ligand **HL1**.

Bond lengths (Å)		Bond angle (°)	
S(1)–C(10)	1.673(2)	O(1)–C(1)–N(1)	127.2(2)
O(1)–C(1)	1.236(3)	O(1)–C(1)–C(2)	126.1(2)
N(2)–N(3)	1.349(3)	N(2)–C(2)–C(1)	127.0(2)
N(2)–C(2)	1.300(3)	N(2)–N(3)–C(10)	121.9(2)
N(3)–C(10)	1.375(3)	N(3)–C(10)–S(1)	123.67(18)
N(4)–C(10)	1.333(3)	N(4)–C(10)–S(1)	123.44(19)
C(1)–C(2)	1.505(3)	Torsional angle (°)	
		O(1)–C(1)–C(2)–N(2)	−3.1(4)
		N(2)–N(3)–C(10)–S(1)	11.1(3)
		N(2)–N(3)–C(10)–N(4)	−170.5(2)

coordination with Cu(II) ion and hence the thiosemicarbazone (**HL1**) act as mono-anionic ONS pincer type ligand, further evidenced by an increment of the C10—S1 bond length [1.673 (**L1**) and 1.728 (1)]. This indicates the thiolate coordination of sulphur. The crystal data of **1** further shows an intermolecular hydrogen bonding between the indole N—H of a molecule and carbonyl oxygen and chlorine of another molecule in the crystal lattice (Table S3).

2.4. DNA binding studies

Deoxyribonucleic acids (DNA) are the vital cellular components, which contain the instructions in the form of base sequences for the life process such as cell survival, proliferation and other biological processes. Transitions of the sequences enable the synthesis of proteins which are found in many forms (hormones, enzymes, structural proteins, etc.), executing all body process. Hence any changes to the DNA nature can alter the normal cell activities and can prevent the cell multiplications. This makes the DNA as the pharmacological target for various drugs, especially for anticancer agents involving the metal ions, hence the investigation of the interacting ability of metal complexes with DNA is extremely significant for the development of therapeutic agent with great medicinal value. Small molecules can interact with DNA in different ways such as (i) intercalation to adjacent base pairs; (ii) electrostatic binding to the sugar-phosphate backbone of the DNA helix; (iii) groove binding (iv) the covalent binding of metal complexes to the nitrogen atoms of bases pairs of DNA [41]. The type and extent of binding of complexes (**1–3**) to CT-DNA were studied by different techniques.

2.4.1. Electronic absorption titration

The UV–Vis absorption spectroscopy is an effective way to analyse the binding affinity and interaction mode of metal complexes with DNA. The complexes (**1–3**) showed absorption bands in the range of 416–422 nm. Upon the titration of CT-DNA with the complexes **1–3**, a significant decrease in molar absorptivity (hypochromism) with a slight towards longer wavelength (redshift) was observed (Figs. 3a and S13). The above observations are generally associated with intercalative mode of interaction involving a strong stacking interaction between the base pairs of the DNA and the aromatic chromophore present in the complexes [42]. Also, the strength of interaction of metal complexes with DNA can be correlated to the observed hypochromism. For the complexes **1–3,** the order of hypochromism was observed as **1** > **2** > **3,** which indicate that the complex **1** have higher affinity and complex **3** showed the least interaction. In order to obtain the quantitative comparison of DNA interaction, the binding constant (K_b) of the complexes were calculated by examining the UV–Vis spectral data with Eq. (1) [43].

$$[DNA]/(\varepsilon_a - \varepsilon_f) = [DNA]/(\varepsilon_b - \varepsilon_f) + 1/K_b(\varepsilon_b - \varepsilon_f) \quad (1)$$

where

Table 3
Selected bond lengths (Å), angles (°) of complex **1**.

Bond lengths (Å)		Bond angles (°)		Torsional angles (°)	
Cu(1)–Cl(1)	2.241(2)	Cl(1)–Cu(1)–S(1)	100.98(9)	Cu(1)–S(1)–C(10)–N(3)	–4.3(8)
Cu(1)–S(1)	2.273(2)	Cl(1)–Cu(1)–O(3)	98.26(15)	Cu(1)–S(1)–C(10)–N(4)	177.2(6)
Cu(1)–O(1)	2.103(6)	O(1)–Cu(1)–Cl(1)	91.39(16)	Cu(1)–O(1)–C(2)–N(2)	–176.9(7)
Cu(1)–O(3)	2.250(5)	O(1)–Cu(1)–S(1)	162.68(17)	Cu(1)–O(1)–C(2)–C(1)	3.8(9)
Cu(1)–N(1)	1.989(7)	N(1)–Cu(1)–O(1)	82.1(3)	Cu(1)–N(1)–N(3)–C(10)	5.4(9)
S(1)–C(10)	1.728(9)	O(1)–Cu(1)–O(3)	84.2(2)	Cu(1)–N(1)–C(1)–C(2)	–3.4(9)
O(1)–C(2)	1.258(10)	O(3)–Cu(1)–S(1)	105.64(15)	Cu(1)–N(1)–C(1)–C(4)	178.4(8)
N(1)–N(3)	1.336(9)	N(1)–Cu(1)–Cl(1)	164.6(2)	N(1)–N(3)–C(10)–S(1)	0.3(10)
N(1)–C(1)	1.292(11)	N(1)–Cu(1)–S(1)	82.9(2)	N(1)–N(3)–C(10)–N(4)	178.9(7)
N(3)–C(10)	1.377(11)	N(1)–Cu(1)–O(3)	95.0(3)	N(1)–C(1)–C(2)–O(1)	–0.5(11)
N(4)–C(10)	1.323(10)	O(3)–Cu(1)–S(1)	105.64(15)	N(1)–C(1)–C(2)–N(2)	–180.0(7)

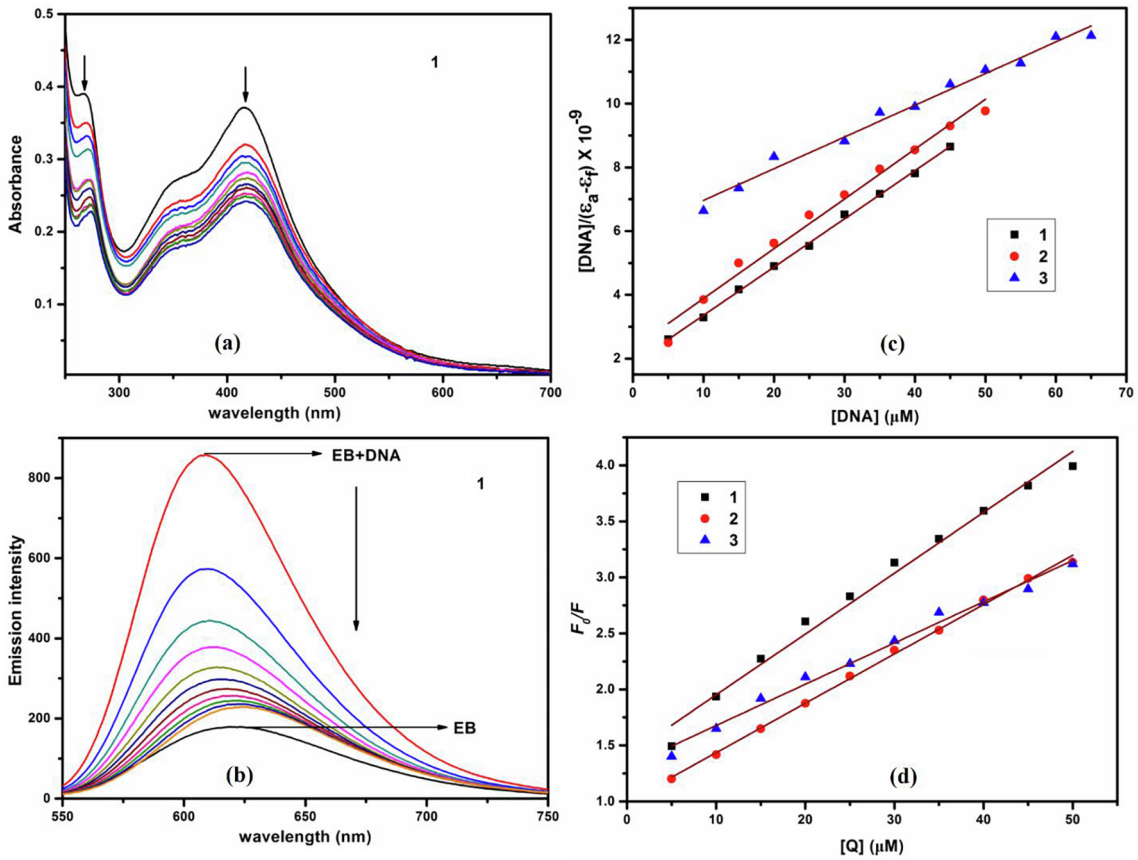

Fig. 3. (a) Absorption spectra of complex **1** up on the titration of CT-DNA. The arrow indicates the absorption intensity decrease upon incremental addition of DNA. (b) Emission spectra of EB bound DNA system with the incremental addition of complex **1**. (c) The plots of $[DNA]/(\varepsilon_a - \varepsilon_b)$ versus $[DNA]$ for the titration of CT-DNA with the complexes **1–3**. (d) Stern-Volmer plots of fluorescence titrations of the complexes (**1–3**) with CT-DNA.

$[DNA]$ = is the concentration of DNA in base pairs
ε_a = the apparent molar absorption coefficient value obtained as $A_{(observed)}/[complex]$
ε_f = the molar absorption coefficient of the free compound
ε_b = the molar absorption coefficient of the compound in the fully bound form.

The intrinsic binding constants K_b for complexes were obtained as the ratio of slope $[1/(\varepsilon_b - \varepsilon_f)]$ to the intercept $[1/K_b(\varepsilon_b - \varepsilon_f)]$ of the he plot $[DNA]/(\varepsilon_a - \varepsilon_b)$ versus $[DNA]$ (Fig. 3c). The values of (K_b) are given in Table 4. The observed values of K_b revealed that the complex **1** shows higher binding affinity than **2** and **3**. It may be due to the fact that the pyrrolidine substituted **L1** of **1** is least polar and hence more hydrophobic compared to the **L2** (2) and **L3** (3), which has morpholine and cyclohexyl substitution respectively. The oxygen atom on the morpholine moiety of **L2** which increase the polarity of the molecule and the terminal N-H on the **L3** which helps for hydrogen bonding will enhance the hydrophilicity. Since the hydrophobic group interact more strongly to the hydrophobic region (base pairs) of DNA complex **1** shows higher interaction.

Table 4
DNA binding constant (K_b), Stern-Volmer constant (K_q) and the apparent binding constant (K_{app}) for complexes **1–3**.

Complex	$K_b(M^{-1})$	$K_q(M^{-1})$	$K_{app}(M^{-1})$
1	$(0.82 \pm 0.09) \times 10^5$	$(5.38 \pm 0.18) \times 10^4$	$(5.03 \pm 0.19) \times 10^6$
2	$(0.69 \pm 0.06) \times 10^5$	$(4.33 \pm 0.13) \times 10^4$	$(3.31 \pm 0.23) \times 10^6$
3	$(0.18 \pm 0.02) \times 10^5$	$(3.47 \pm 0.10) \times 10^4$	$(2.61 \pm 0.14) \times 10^6$

2.4.2. Fluorescence spectroscopic studies

EB (Ethidium bromide) displacement test was also done to recognise the mode of metal complexes-DNA interaction. EB emits intense fluorescence when it binds to CT-DNA due to the strong hydrophobic interaction of EB through intercalation between the base pairs of DNA. If a molecule competitively binds to DNA, the molecule will displace the bound EB from base pairs, will causes quenching in the fluorescence of EB. The magnitude of quenching of fluorescence reflects the extent of interaction with the added molecule. The fluorescent intensity of DNA bound EB was recorded in the absence and the incremental addition of **1–3** (Fig. 3b and S14). The addition of the complexes (**1–3**) caused a noticeable reduction in emission intensity, which indicate the binding of the complexes to DNA by replacing the EB. In order to find out the relative binding ability complexes to CT-DNA with respect to EB, the observed data were analysed with the help of the Stern-Volmer equation (Eq. (2)) [44].

$$F_0/F = 1 + K_q[Q] \quad (2)$$

where F_0 and F are the fluorescence intensities with and without presenc of the complex respectively, K_q is the linear Stern-Volmer quenching constant, and $[Q]$ is the complex concentrations. The slope of the plot of F_0/F versus $[Q]$ gave the $K_q$value. The Stern-Volmer plot (Fig. 3d) illustrate that, the fluorescnt quenching of EB-DNA system by **1–3** is linear in nature. From K_q values, it is clear that complex **1** have higher quenching constant and the order of the magnitude of K_q is **1 > 2 > 3,** and is similar to the result from absorption spectral studies. The apparent DNA binding constant (K_{app}) values were also calculated with the equation,

$$K_{EB}[EB] = K_{app}[compound] \quad (3)$$

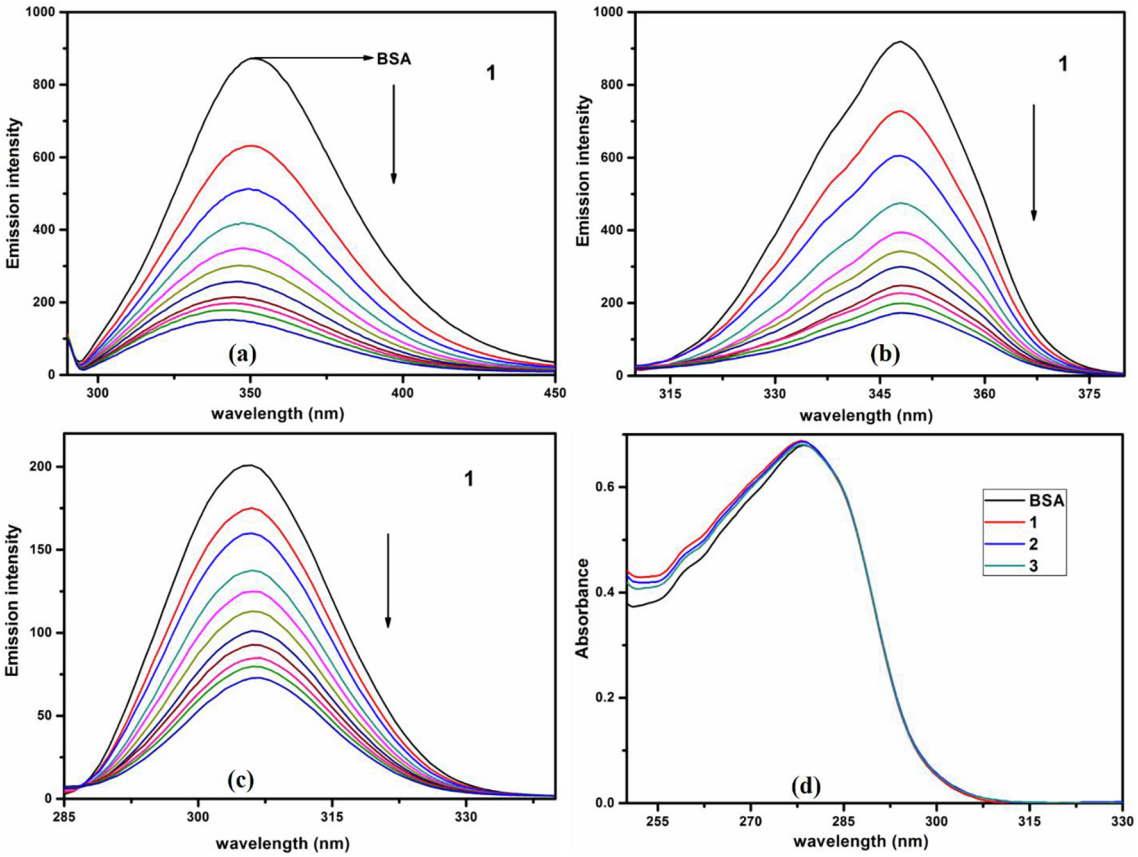

Fig. 4. (a) Emission spectrum of BSA with the incremental addition of complex **1**. (b) Synchronous spectra of BSA up on the titration of complex **1** and Δλ = 60 nm. (c) Synchronous spectra of BSA up on the titration of complex **1** and Δλ = 15 nm. {For (a), (b) and (c) the [BSA] = 1 μM and [complex] = 0–20 μM}. (d) The absorption spectra of BSA (1 μM) and BSA with **1–3** (5 μM).

where [*compound*] is the concentration complexes required to reduce 50% initial fluorescence intensity of EB, $K_{EB} = 1.0 \times 10^7\ M^{-1}$ and [*EB*] = 5 μM. The quenching constant (K_{EB} and K_{app}) values are listed in Table 4

2.5. Protein binding studies

Protein interaction studies of **1–3** were performed with Bovine serum albumin (BSA). Intensity changes and shifts in the wavelength of both UV–Vis and fluorescent spectra of BSA were analysed in the presence and the absence of complexes **1–3**.

2.5.1. Absorption studies

UV–Visible absorption spectra of BSA was recorded with complexes to understand the mechanism of quenching process (Fig. 4d). As shown in Fig. 4d, there was no significant changes in absorption spectra of BSA after the addition of complexes. This indicates that, the kind of interaction between Cu(II) complexes (**1–3**) and BSA was mainly a dynamic quenching process [40].

2.5.2. Fluorescence studies

The intrinsic fluorescence of proteins is sensitive in nature due to the high sensitivity of fluorophore to its local environment which may change with conformational changes, association and dissociation of subunits and denaturation. Hence the emission spectra of proteins can provide useful information on their structure and mechanism and are frequently utilised in protein folding and association reactions. Hence, fluorescence spectroscopy is one of the key technique to investigate the interactions of metal complexes with BSA

To study the interactions of complexes Cu(II) (**1–3**) with BSA, the emission spectra of BSA recorded in the range of 285–500 nm by exciting the BSA (1 μM) at 280 nm with increasing concentration (0–20 μM) of the complexes (**1–3**). Fig. 4a shows the representative fluorescence emission spectra of BSA after the addition of complex **1**. As the figure shows, the incremental addition of the complexes **1–3** caused a substantial decline in the fluorescence intensity of BSA at 345–350 nm region with a blue shift of 6–8 nm for all complexes. The percentage of decrease was found as 82%, 75% and 78% from the initial intensity of BSA, respectively for **1**, **2** and **3**. The observed hypochromism and blue shift suggesting the interactions of added metal complexes with BSA and affecting its conformation which in turn causing the changes in the local environment of the fluorophore. The extent of fluorescence quenching was calculated in terms of quenching constant (K_q) is described by the Stern-Volmer relation (Eq. (2), Fig. 5a). The binding ability of complexes were also evaluated in terms of binding constant (K_b) using the Scatchard equation (Eq. (4)), which represent the equilibrium among bound and free molecules of the system in which ligands bind independently to a set of similar sites on a macromolecule.

$$\log[(F_0 - F)/F] = \log K_b + n\log[Q] \quad (4)$$

The number of binding sites (n) and the binding constant (K_b) values were calculated from the plot of $\log[(F_0 - F)/F]$ versus $\log[Q]$ (Fig. 5b). The (K_q), (K_b) and (n) values for the interactions of the **1–3** with BSA are shown in Table 5. The result suggested that, all complexes showing good interactions in which complex **1** have a higher binding affinity. Based on the K_b and K_q values, the affinity of the complexes (**1–3**) to the BSA follows the order **1–3** > **2**. The ***n*** value suggest the presence of mono binding site in BSA for all the complexes.

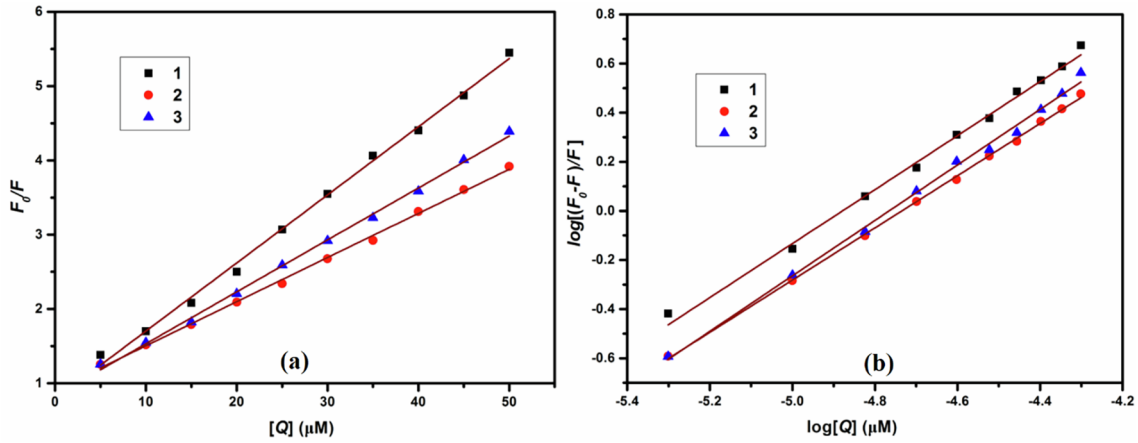

Fig. 5. (a) Stern-Volmer plots of fluorescence titrations of complexes **1–3** with BSA. (b) Scatchard plots of fluorescence titrations of complexes **1–3** with BSA.

Table 5
Binding constant (K_b), quenching constant (K_q) and number of binding sites (n) for the interaction of complexes **1–3** with BSA.

Complex	$K_b(M^{-1})$	$K_q(M^{-1})$	n
1	$(2.29 \pm 0.15) \times 10^5$	$(9.47 \pm 0.31) \times 10^4$	1.09
2	$(1.13 \pm 0.08) \times 10^5$	$(6.21 \pm 0.17) \times 10^4$	1.06
3	$(2.43 \pm 0.23) \times 10^5$	$(7.18 \pm 0.33) \times 10^4$	1.13

2.5.3. Synchronous fluorescence spectroscopic studies

Synchronous fluorescence spectroscopy (SFS) have a crucial role in the analysis of the multicomponent sample. It has the significant advantage of improved selectivity, reduction in light scattering and spectral simplification [45]. Hence SFS can be used for the specific analysis of tryptophan and tyrosine fluorescence spectra of BSA to better understand the changes in the microenvironment around this fluorophore and hence the conformational changes to the BSA during the addition of metal complexes. The constant-wavelength SFS (CWSFS) was used here. In CWSFS, a wavelength difference ($\Delta\lambda$) between the excitation (λ_{ex}) and emission (λ_{em}) wavelength were kept constant during the simultaneous scanning of excitation and emission monochromators. The $\Delta\lambda$ echoes the nature of the chromophore [32]. Hence the $\Delta\lambda = 60$ nm and $\Delta\lambda = 15$ nm is the characteristic of tryptophan and tyrosine residue respectively. After the addition of the complexes, the fluorescence intensity of both the tryptophan (at 350 nm) and tyrosine (at 310 nm) was decreased (Fig. 4b, c, S16 and S17). Hence the SFS studies suggested that the interaction of complexes (**1–3**) influenced the local environment of both tryptophan and tyrosine of BSA, which indicate the conformational changes of BSA during the interaction with metal complexes **1–3**.

2.6. Biological activities

2.6.1. Antibacterial activity

The *in vitro* antibacterial activity of **HL1**-**HL3** and its metal complexes **1–3** were tested against sensitive organisms such as *Staphylococcus Aureus*, *Bacillus Subtilis* and *Staphylococcus Epidermidis* (Gram-positive), *Escherichia Coli*, *Pseudomonas aeruginosa* and *Proteus Vulgaris* (Gram-negative) bacterial strains by disc diffusion method [46,47] and Ciprofloxacin as a positive control. The minimum inhibitory concentration (MIC) values for the compounds under test and standard were reported in μg/mL and the results are tabulated in Table 6. It is evident from Table 6 that the complex **3** has shown potent efficacy with broad-spectrum activity against *S. aureus* (MIC: 8.56 μg/mL), *B. subtilis* (MIC: 10.35 μg/mL), *S. epidermidis* (MIC: 6.50 μg/mL), *P. aeruginosa* (MIC: 21.36 μg/mL) and *P. vulgaris* (MIC: 17.64 μg/mL), respectively compared to the standard drug. Similarly, complex **2** has shown good inhibition against *S. epidermidis* (MIC: 5.37 μg/mL) and *P. vulgaris* (MIC: 18.63 μg/mL). Complex **1** and **HL1** shown moderate activity against *E. coli* and *S. aureus* have respectively with respective MIC values of 35.75 μg/mL and 25.19 μg/mL. Remaining compounds have shown poor activity against all the tested strains.

2.6.2. Antifungal activity

All the compounds were evaluated against five selected strains such as *Aspergillus niger*, *Aspergillus flavus*, *Fusarium solani*, *Candida albicans* and *Curvularia lunata*. Nystatin was chosen as a standard drug. The MIC (μg/mL) of the tested compounds results are presented in Table 7. The antifungal activity results revealed that in all the compounds, complex **3** has shown notable activity against *A. niger* (MIC: 11.67 μg/mL), good activity against *A. flavus*, *C. albicans* and *C. lunata* (MIC: 8.14 μg/mL, 17.56 μg/mL and 14.38 μg/mL, respectively) and poor activity against *F. solani*. The complex **1** has shown good activity *C. albicans* and moderate activity against *A. flavus* and *F. solani* (MIC: 16.94 μg/mL, 11.53 μg/mL and 16.52 μg/mL) compared to standard Nystatin. Remaining all the compounds have exhibited moderate to poor activity with MIC ranging from 21.93 μg/mL to 71.53 μg/mL.

2.6.3. Scavenging activity

The newly synthesized complexes (**1–3**), were subjected for their *in vitro* radical scavenging activity in terms of hydrogen donating or radical scavenging ability by DPPH (1,1-diphenyl-2-picrylhydrazyl) method [48]. The results were expressed in μM and ascorbic acid was considered as reference drug (Table 8, Fig. 6). All the complexes showed radical scavenging activity with IC_{50} values ranging from 19.23 ± 1.05 μM to 35.17 ± 0.55 μM. Among all the complexes, complex **1** has shown good scavenging (IC_{50}: 19.23 ± 1.05 μM) compared to standard ascorbic acid. Complex **2** has shown moderate activity and complex **3** shown poor activity with IC_{50} values of 27.01 ± 1.93 μM and 35.17 ± 0.55 μM. Based on the above results the order of activity is **1** > **2** > **3**.

2.6.4. In vitro anti-proliferative activity:

The *in vitro* anti-proliferative activity of the complexes (**1–3**) was evaluated for different cancer [MCF-7 (breast), A549 (lung) and HeLa (cervical)] cell lines. The percentage of cell viability versus concentration graph is shown in Fig. 7. The half minimum inhibitory concentration (IC_{50}) values of the complexes are tabulated (Table 9). The activity results revealed that complex **1** has exhibited broad-spectrum activity against MCF-7, A549 and HeLa with IC_{50} value 14.83 ± 0.45 μM, 17.88 ± 0.16 and 6.89 ± 0.42 μM, respectively which was comparable to that of the standard Doxorubicin. Similarly, complex **3** against MCF-7 shown moderate activity (IC_{50}: 25.02 ± 0.51 μM) and the remaining complexes against all the cell

Table 6
Antibacterial activity of the synthesized compounds (MIC, μg/mL).

Compound	*S. aureus*	*B. subtilis*	*S. epidermidis*	*E. coli*	*P. aeruginosa*	*P. vulgaris*
L1	25.19	> 150	51.94	47.58	> 150	> 150
L2	61.75	> 150	> 150	> 150	75.91	> 150
L3	> 150	47.26	> 150	63.45	45.57	> 150
1	> 150	29.81	18.39	35.75	> 150	38.60
2	> 150	> 150	5.37	50	> 150	18.63
3	8.56	10.35	6.50	39.28	21.36	17.64
Ciprofloxacin	**6.25**	**6.25**	**3.12**	**12.5**	**12.5**	**12.5**

Table 7
The antifungal activity of the compounds (MIC, μg/mL).

Compound	*A. niger*	*A. flavus*	*F. solani*	*C. albicans*	*C. lunata*
L1	> 150	71.53	27.80	> 150	36.79
L2	50	65.74	> 150	39.26	50
L3	43.51	> 150	> 150	36.51	50
1	> 150	11.53	16.52	16.94	> 150
2	21.93	> 150	> 150	> 150	37.61
3	11.67	8.14	50	17.56	14.38
Nystatin	**4.75**	**2.81**	**3.28**	**4.16**	**3.12**

Table 8
Radical scavenging activity of the newly synthesized compounds (**1–3**) by DPPH scavenging assay.

Compound	IC_{50} (μM)
1	19.23 ± 1.05
2	27.01 ± 1.93
3	35.17 ± 0.55
Ascorbic acid	**6.13 ± 0.43**

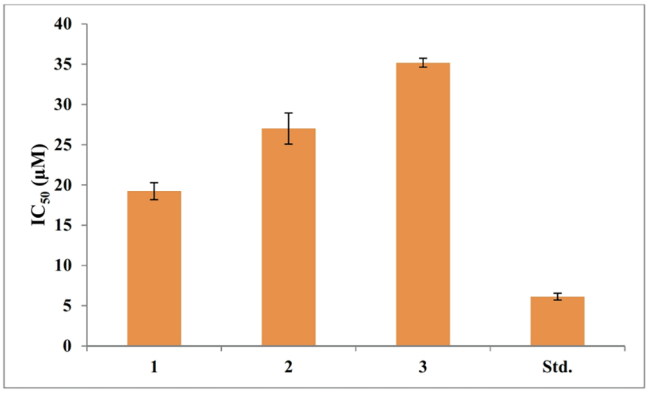

Fig. 6. Radical scavenging activity of the newly synthesized complexes (**1–3**).

lines were exhibited less activity IC_{50} ranging from 10.86 ± 0.65 μM to 64.97 ± 1.06 μM. We have also tested for anti-proliferative activity against normal HEK-293 (Embryonic Kidney 293) cell line and the results are tabulated in Table 9.

3. Conclusion

The thiosemicarbazone derivatives of 5-methoxy isatin, differentiated by different N-terminal substitutions (**HL1**, Pyrrolidine; **HL2**, Morpholine and **HL3**, Cyclohexyl) and their copper(II) complexes (**1–3**) have been synthesised and characterised with an aim to assess their biological applications and the effect of terminal N-substitution on biological activity. The crystal data and molecular structure of the ligand **HL1** and complex **1** was established by single crystal X-ray diffraction method. The UV–Vis and fluorescent spectroscopic investigation on DNA interacting capability of complexes **1–3** showed the ability

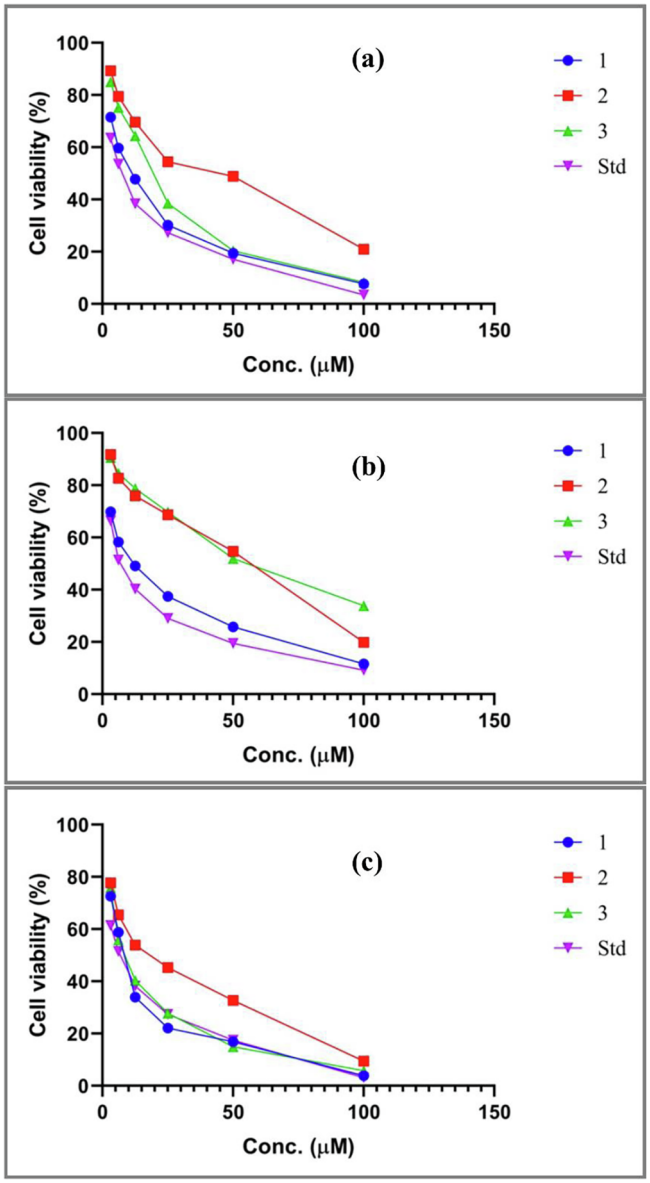

Fig. 7. Dose response curves of complexes **1–3** against (a) **MCF-7** cell lines, (b) **A-549** cell lines and (c) **HeLa** cell lines.

of the complexes to interact with DNA, mainly through the intercalative mode. The binding parameters such as K_b, K_q, K_{app} suggesting that, each complexes have a different activity, in which complex **1** have higher affinity. The complexes **1–3** were also showed their ability to interact with BSA protein and influence its confirmation, again the effect of complex **1** is better than that of complex **2** and **3**. The higher activity of **1** can be attributed to its higher hydrophobic nature compare to **2** and **3,** so the complex **1** can more effectively interact with the hydrophobic

Table 9
The *in vitro* anticancer activity of compounds **1–3** on human cancer cell lines (IC_{50} in μM).[a]

Compound	MCF-7	A549	HeLa	HEK 293
1	14.83 ± 0.45	17.88 ± 0.16	6.89 ± 0.42	90.85 ± 2.31
2	49.38 ± 0.16	55.52 ± 0.63	28.79 ± 0.32	94.53 ± 1.22
3	25.02 ± 0.51	64.97 ± 1.06	10.86 ± 0.65	72.16 ± 1.25
Doxorubicin	**3.47 ± 0.31**	**4.69 ± 0.25**	**1.29 ± 0.17**	ND

[a] Values are stated as mean ± SEM. Cytotoxicity as IC_{50} for each cell line, is the concentration of compound required to reduce the optical density of treated cells to 50% with respect to untreated cells using the MTT assay. ND = Not Done.

centres of both DNA and BSA. For BSA interaction studies, both complex **1** and **3** almost similar activity. I may be due to the possible hydrogen bonding interactions between the amino acids of proteins and hydrogen present in 4N position of HL3 ligand. The antibacterial study has shown that each complexes have a different range of activity. The complex **3** has shown potent activity against three gram positive bacteria such as *S. aureus*, *B. subtilis* and *S. epidermidis*, two gram negative bacteria *P. aeruginosa* and *P. vulgaris* while complex **2** showed activity towards *S. epidermidis* and *P. vulgaris*. In case of antifungal activity the complex **3** has shown promising activity against *A. niger* and *A. flavus*. The radical scavenging study indicates that, all complexes showed the scavenging activity and the order of activity is **1** > **2** > **3**. The *in vitro* anticancer activity of synthesized complexes on human cancer cell lines (MCF-7, A549, HeLa) have also been investigated, the results are showing that the complexes **1–3** have the ability to inhibit the growth of cancer cells. Further the complexes showed some selective nature towards various cell lines, in which complex **1** showed more potent nature towards all three cancer cell lines. Complex **2** showed more activity towards HeLa cell lines. The more active complex **1** was also studied against HEK 293 as a demonstrative of normal cell line. The result showed that, it is less toxic towards normal cell line. Compared to DNA/BSA interaction studies, other biological studies did not follow a particular order. Which indicates the possibilities of other mechanistic pathways and factors, and need to be studied further in order to fully understand the structural activity of different 4N-substituted thiosemicarbazone and its complexes. Finally, the synthesised thiosemicarbazone series and their complexes which are only differed by N-terminal substitution of thiosemicarbazone ligand showed different level of activities towards various biological studies. So the whole studies signifying the influence of the substitution at the N-terminal position of thiosemicarbazones which gives us more option to further tune and enhance the activity thiosemicarbazones and their metal complexes.

4. Experimental section

4.1. Materials and methods

Chemicals and solvents for the experiments were purchased from Alfa Aesar/Merck/Sigma-Aldrich, and were used as received. Lab India instrument was used to record the melting points of the compounds and are uncorrected. Elemental analysis was carried out with a Vario EL-III CHNS analyser. The FT-IR spectra of **HL1**-**HL3** and **1–3** were recorded by the PerkinElmer Frontier FT-IR/FIR spectrometer. Analytikjenaspecord S 600 UV–Vis spectrophotometer was used to perform the electronic absorption studies. Emission spectra were recorded using Jasco FP–8300 Fluorescent spectrophotometer. NMR studies were carried out in DMSO-d_6 solvent on a Bruker 500 MHz instrument. The ESI mass spectra of the ligands and complexes were recorded using THERMO exactive orbitrap mass spectrometer. EPR spectra were recorded on a JES-X3 Series EPR instrument at liquid nitrogen temperature and operating at X-band frequency (9.1 GHz).

4.2. Synthesis of ligands

Pyrrolidine-1-carbothiohydrazide, morpholine-4-carbothiohydrazide, 4-Cyclohexyl-3-thiosemicarbazide were synthesized according to the literature [49,50]. The ligands (**HL1**-**HL3**) were synthesized by refluxing an ethanolic mixture of 5-methoxyindoline-2,3-dione and appropriate carbothiohydrazide in the presence of 1 drop of conc. H_2SO_4. The reaction was monitored by TLC. After 4 h, the resultant product was filtered, washed and dried [51].

4.2.1. (Z)-N-(5-methoxy-2-oxoindolin-3-ylidene)pyrrolidine-1-carbothiohydrazide (HL1)

Pyrrolidine-1-carbothiohydrazide (0.145 g, 0.001 mol), 5-methoxyindoline-2,3-dione were (0.177 g, 0.001 mol) were used. Orange coloured powder, yield: 81%. M.p.: 245 °C. Anal. Calcd. $C_{14}H_{16}N_4O_2S$ (%): C, 55.25; H, 5.30; N, 18.41; S, 10.53. Found: C, 55.37; H, 5.41; N, 18.21; S, 10.28. UV–Vis (DMSO): λ_{max} (nm) 287, 347. FT-IR (ATR): υ (cm^{-1}) 3453 (N−H isatin), 3200 (N−H), 1667 (C=N), 1693 (C=O), 1341 (C=S). ^{1}H NMR (500 MHz, DMSO-d_6): δ, ppm 13.64 (s, 1H), 11.13 (s, 1H), 7.69–6.87 (m, 3H), 3.42 (s, 3H), 3.78–3.72 (d, 4H), 2.09–1.90 (m, 4H). ^{13}C NMR (125 MHz, DMSO-d_6): δ, ppm 176.1 (C=S); 163.57 (C = 0); 152.4 (C=N); 135.95, 134.85, 121.45, 117.44, 112.33, 105.72 (aromatic carbons); 56.10 (O–CH_3); 53.70, 49.68, 26.31, 24.17 (aliphatic carbons). ESI-MS (*m/z*) = 305.12 $[M+1]^+$.

4.2.2. (Z)-N-(5-methoxy-2-oxoindolin-3-ylidene)morpholine-4-carbothiohydrazide (HL2)

Morpholine-4-carbothiohydrazide (0.161 g, 0.001 mol), 5-methoxyindoline-2,3-dione (0.177 g, 0.001 mol) were used. Orange-red-coloured powder, yield: 80%. M.p.: 260 °C. Anal. Calcd. $C_{14}H_{16}N_4O_3S$ (%): C, 52.49; H, 5.03; N, 17.49; S, 10.01. Found: C, 52.72; H, 5.29; N, 17.37; S, 9.73. UV–Vis (DMSO): λ_{max} (nm) 305, 369. FT-IR (ATR): υ (cm^{-1}) 3475 (N−H isatin), 3281(N−H), 1628 (C=N), 1701 (C=O), 1348 (C=S).^{1}H NMR (500 MHz, DMSO-d_6): δ, ppm 13.30 (s, 1H), 11.15 (s, 1H), 7.05–6.37 (m, 3H), 3.41 (s, 3H), 4.01–3.75 (m, 8H).^{13}C NMR (125 MHz, DMSO-d_6): δ, ppm 179.82 (C=S); 163.18(C=O); 155.44 (C=N); 136.43, 135.16, 121.21, 117.92, 122.39, 105.94 (aromatic carbons); 56.33 (O–CH_3); 66.19, 50.42 (aliphatic carbons). ESI-MS *m/z* = 321.10 $[M+1]^+$.

4.2.3. (Z)-N-cyclohexyl-2-(5-methoxy-2-oxoindolin-3-ylidene) hydrazinecarbothioamide (HL3)

4-Cyclohexyl-3-thiosemicarbazid (0.173 g, 1 mmol), 5-methoxyindoline-2,3-dione (0.177 g, 1 mmol) were used. Red coloured powder, yield: 83%. M.p.: 252 °C. Anal. Calcd. $C_{16}H_{20}N_4O_2S$ (%): C, 57.81; H, 6.06; N, 16.85; S, 9.64. Found: C, 57.98; H, 5.98; N, 16.69; S, 9.73. UV–Vis (DMSO): λ_{max} (nm) 304, 381. FT-IR (ATR): υ(cm^{-1}) 3373 (N−H isatin), 3204(N−H), 1622 (C=N), 1692 (C=O), 1349 (C=S).^{1}H NMR (500 MHz, DMSO-d_6): δ, ppm 12.71 (s, 1H), 10.34 (s, 1H), 8.29 (s, 1H), 7.27–6.30 (m, 3H), 3.81 (s, 3H), 2.56–1.24 (m, 12H). ^{13}C NMR (125 MHz, DMSO-d_6): δ, ppm 176.59 (C=S); 163.02 (C=O); 155.51 (C=N); 136.49, 132.18, 121.18, 117.14, 111.99, 106.90 (aromatic carbons); 56.13 (O–CH_3); 40.27, 32.15, 25.21(aliphatic carbons). ESI-MS (*m/z*) = 333.13 $[M+1]^+$.

4.3. Synthesis of copper(II) complexes (1–3)

The ethanolic solution of $CuCl_2{\cdot}2H_2O$ (1 mmol) was added into the solution of appropriate ligands (1 mmol) in ethanol. The reaction mixture was stirred for 5 h under reflux, and then the precipitate formed was filtered, washed and dried.

4.3.1. Bis[(Z)-N-(5-methoxy-2-oxoindolin-3-ylidene)pyrrolidine-1-arbothiohydrazide] Cu(II) (1)

Brown coloured powder, yield: 80%. M.p.: 281 °C. Anal. Calcd. $C_{14}H_{15}ClCuN_4O_2S$ (%): C, 41.79; H, 3.76; N, 13.92; S, 7.97. Found: C,

41.98; H, 3.81; N, 13.79; S, 7.59. UV–Vis (DMSO): λ_{max} (nm) 269, 352, 416, 635(DRS). FT-IR (ATR): υ(cm^{-1}) 3305 (N—H isatin), 1572 (C═N), 1656 (C═O), 1326 (C═S). EPR (LNT): 'g' values ($g_{\parallel}$, $g_{\perp}$) 2.214, 2.043. ESI-MS (*m/z*) = 400.04 $[M]^+$, 401.05 $[M+1]^+$

4.3.2. Bis[(Z)-N-(5-methoxy-2-oxoindolin-3-ylidene)morpholine-4-carbothiohydrazide] Cu(II) (2)

Brown coloured powder, yield: 82%. M.p.: 293 °C. Anal. Calcd. $C_{14}H_{15}ClCuN_4O_3S$ (%): C, 40.19; H, 3.61; N, 13.39; S, 7.66. Found: C, 40.31; H, 3.71; N, 13.31; S, 7.37. UV–Vis (DMSO): λ_{max} (nm) 265, 376, 417, 639(DRS). FT-IR (ATR): υ(cm^{-1}) 3231 (N—H isatin), 1592 (C═N), 1649 (C═O), 1332 (C═S). EPR (LNT): 'g' values ($g_{\parallel}$, $g_{\perp}$) 2.217, 2.051. ESI-MS (*m/z*) = 417.04 $[M]^+$, 382.02 $[M-Cl]^+$.

4.3.3. Bis[(Z)-N-cyclohexyl-2-(5-methoxy-2-oxoindolin-3ylidene) hydrazinecarbothioamide] Cu(II) (3)

Brown coloured powder, yield: 85%. M.p.: 301 °C. Anal. Calcd. $C_{16}H_{19}ClCuN_4O_2S$ (%): C, 44.65; H, 4.45; N, 13.02; S, 7.45. Found: C, 44.87; H, 4.53; N, 12.93; S, 7.21. UV–Vis (DMSO): λ_{max} (nm) 267, 366, 417, 610(DRS). FT-IR (ATR): υ(cm^{-1}) 3313 (N—H isatin), 1545 (C═N), 1663 (C═O), 1340 (C═S), . EPR (LNT): 'g' values ($g_{\parallel}$, $g_{\perp}$) 2.219, 2.039. ESI-MS (*m/z*) = 429.07 $[M]^+$, 430.06 $[M+1]^+$.

4.4. Single crystal X-ray diffraction studies

The suitable crystals for the diffraction studies were obtained from DMSO/methanol solution.

The detailed explanations of the experiments are given in the supplementary information file.

4.5. DNA interaction studies

4.5.1. Electronic absorption studies

The interaction studies of complexes (**1**–**3**) with CT-DNA were performed in Tris HCl/NaCl buffer (pH 7.2). The buffer was prepared by dissolving tris(hydroxymethyl) aminomethane (Tris, 5 mM) and sodium chloride (50 mM) in double distilled water and adjusted to pH 7.2 with diluted hydrochloric acid. The stock solution of CT-DNA was prepared by dissolving the CT-DNA in Tris HCl/NaCl buffer. The purity of the calf thymus DNA was verified by taking absorption ratio of CT DNA solutions at λ_{max} 260 and 280 nm, and the ratio was found to be 1.87, indicating that DNA was sufficiently protein free [52]. The DNA concentration was decided using UV–Visible absorbance and monitoring the molar absorption coefficient (6600 $M^{-1}cm^{-1}$) values at 260 nm [53]. The solution of metal complexes with required concentration were prepared in 5% DMSO/Tris HCl/NaCl solution. The absorption titration was performed with incremental addition of CT-DNA (5–50 μM) to a fixed concentration of (25 μM) complex solution in the cuvette. An equal amount of DNA was also added to the reference solution to avoid the absorbance of DNA itself.

4.5.2. Fluorescent titration studies

The quenching constant (K_q) and apparent binding constant (K_{app}) values of the complexes (**1**–**3**) were determined by a ethidium bromide (EB) displacement assay using fluorescence spectroscopy. Ethidium bromide solution was prepared in Tris HCl/NaCl buffer (pH 7.2) solution and the DNA was pre-treated with ethidium bromide and then the solutions of complexes were incrementally (0–50 μM) added to this mixture of EB bound DNA solution, and the change in the fluorescence intensities of EB was measured at 605 nm (520 nm excitation).

4.6. Protein binding studies

Fluorescence spectroscopy method was employed to study the binding of the copper thiosemicarbazone complexes (**1**–**3**) with BSA. The stock solution of BSA was prepared in 50 mM phosphate buffer (pH = 7.2). The stock solutions the complexes were prepared in DMSO-phosphate buffer (5:95) solution. The titrations were done by the successive addition of the solution of complexes **1**–**3** (0–20 μM) to a 2.5 mL of BSA solution in the cuvette. The changes in protein nature was monitored by observing the emission spectra of BSA at 345 nm with an excitation wavelength of 280 nm. Synchronous fluorescence spectra was also recorded using the same concentration of BSA and the complexes as mentioned above with two different Δλ (difference between the excitation and emission wavelengths of BSA) values of 15 and 60 nm.

4.7. Biological evaluation

4.7.1. Antimicrobial screening

The in vitro antimicrobial activity of the ligand and its metal complexes were evaluated against gram-negative bacteria such as *Escherichia coli*, *Proteus vulgaris* and *Pseudomonas aeruginosa*, gram positive bacteria like *Staphylococcus aureus* and *Bacillus subtilis* and *Staphylococcus epidermidis,* and few fungal strains such as *Aspergillus niger*, *Aspergillus flavus*, *Fusarium solani*, *Candida albicans* and *Curvularia lunata* by disc diffusion method. Ciprofloxacin and Nystatin were chosen as standards for antibacterial and antifungal activity, respectively. Sterile antibiotic discs (6 mm in diameter, prepared using Whatmann No. 1 paper) were placed over the nutrient agar medium. 100 μg of the compounds (initially dissolved in DMSO) were transferred to each disc with the help of a micropipette. The samples were incubated at 37 °C for 24 h (bacteria) and 25 °C for 48 h (fungi), respectively. The plates were then observed and the inhibition zones were recorded in terms of millimeter.

4.7.2. In vitro cytotoxic bioassay

The synthesized compounds were evaluated for their *in vitro* anticancer activity against five different human cancer cell lines such as HeLa (cervical), MCF-7 (breast), A549 (lung), and HEK293 (embryonic kidney). Cell viability in the presence of the test samples was measured by the MTT-microcultured tetrazolium assay. This assay is a quantitative colorimetric method for the determination of cell viability. The assessed parameter is the metabolic activity of viable cells. Metabolically active cells reduce pale yellow tetrazolium salt (MTT) to a dark blue water-insoluble formazan, which can be directly quantified after solubilisation with DMSO. The absorbance of the formazan directly correlates with the number of viable cells. MCF-7, A549, HeLa and HEK293 cells were plated into a 96-well plate at a density of 1×10^4 cells/well. Cells were grown overnight in the full medium and then switched to the low serum media. 1% DMSO was used as a control. After 48 h of treatment with different concentrations of test compounds, the cells were incubated with MTT (2.5 mg/mL) in the CO_2 chamber for 2 h. The medium was then removed and 100 μL of DMSO was added into each well to dissolve formazan crystals. After thoroughly mixing, the plates were read at 570 nm for optical density, which is directly correlated with cell quantity. The results were represented as percentage of viability. All the experiments were carried out in triplicate.

4.7.3. Antioxidant activity

Free radical scavenging capacity of the metal complexes were determined by using DPPH (1,1-Diphenyl-2-picrylhydrazyl) free radical method described in the literature. Ascorbic acid solution was used as standard. 0.2 mM solution of DPPH was prepared in 100% methanol. The required amount of ascorbic acid was dissolved in 100% methanol to prepare 1 mM solution and the test compounds were dissolved in 0.2% DMSO and methanol to prepare 1 mM stock solutions. From the stock solutions different concentrations (3, 10, 30 and 100 μM) of solutions were prepared on diluting with methanol. 1 mL of each compound solution was added to the 3 mL of DPPH solution. After 30 min, the absorbance of the solutions at 517 nm (A_1) was recorded using UV–Visible spectrophotometer. As a control, the absorbance of the

blank solution of DPPH without test compound was also determined at 517 nm (A_0). The following equation was used for the calculation of the % of scavenging activity.

$$Scavenging\ Activity\ (\%) = \frac{A_0 - A_1}{A_0} \times 100$$

where A_0 is the absorbance of DPPH in the absence of antioxidant and A_1 is the absorbance of DPPH in the presence of antioxidant. IC_{50} values were also calculated for the compounds.

Acknowledgements

KNA and RK thanks to the MHRD, Govt. of India for providing Senior Research fellowship. G. R. thank the Council of Scientific and Industrial Research (CSIR), Govt. of India, for Senior Research Fellowship [(09/895(0006)/2014-EMR-1].

Appendix A. Supplementary data

Supplementary data to this article can be found online at https://doi.org/10.1016/j.ica.2019.04.019.

References

[1] M. Li, Y. Gou, F. Yang, H. Liang, Spectrochim. Acta Part A Mol. Biomol. Spectrosc. 128 (2014) 686–693.
[2] U. Ndagi, N. Mhlongo, M.E. Soliman, Drug Des. Dev. Therapy 11 (2017) 599.
[3] C. Duncan, A.R. White, Metallomics 4 (2012) 127–138.
[4] A. Spassky, D.S. Sigman, Biochemistry 24 (1985) 8050–8056.
[5] P.U. Maheswari, S. Roy, H. den Dulk, S. Barends, G. van Wezel, B. Kozlevcar, P. Gamez, J. Reedijk, J. Am. Chem. Soc. 128 (2006) 710–711.
[6] C. Fernandes, G.L. Parrilha, J.A. Lessa, L.J. Santiago, M.M. Kanashiro, F.S. Boniolo, A.J. Bortoluzzi, N.V. Vugman, M.H. Herbst, A. Horn, Inorg. Chim. Acta 359 (2006) 3167–3176.
[7] B.C. Bales, T. Kodama, Y.N. Weledji, M. Pitie, B. Meunier, M.M. Greenberg, Nucl. Acids Res. 33 (2005) 5371–5379.
[8] L.A. Saryan, E. Ankel, C. Krishnamurti, D.H. Petering, H. Elford, J. Med. Chem. 22 (1979) 1218–1221.
[9] R. Gust, W. Beck, G. Jaouen, H. Schönenberger, Coord. Chem. Rev. 253 (2009) 2742–2759.
[10] Z. Wu, Q. Liu, X. Liang, X. Yang, N. Wang, X. Wang, H. Sun, Y. Lu, Z. Guo, J. Biol. Inorg. Chem. 14 (2009) 1313.
[11] A.C. Sartorelli, B.A. Booth, Cancer Res. 27 (1967) 1614–1619.
[12] B. Ma, B.C. Goh, E.H. Tan, K.C. Lam, R. Soo, S.S. Leong, L.Z. Wang, F. Mo, A.T. Chan, B. Zee, Invest. New Drugs 26 (2008) 169–173.
[13] C. Nutting, C. Van Herpen, A. Miah, S. Bhide, J.-P. Machiels, J. Buter, C. Kelly, D. De Raucourt, K. Harrington, Ann. Oncol. 20 (2009) 1275–1279.
[14] A.B. Miah, K.J. Harrington, S.A. Bhide, C.M. Nutting, C.M.L. van Herpen, J.-P. Machiels, J. Buter, C. Kelly, D. de Raucourt, Ann. Oncol. 20 (2009) 1275–1279.
[15] K. Ga, Br. Med. J. 2 (1964) 621 621.
[16] V. Mishra, S.N. Pandeya, C. Pannecouque, M. Witvrouw, E. De Clercq, Arch. Pharm. 335 (2002) 183–186.
[17] N.D. Thanh, H.T. Duc, V.T. Duyen, P.M. Tuong, N. Van Quoc, Chem. Cent. J. 9 (2015) 60-60.
[18] B.A. Gingras, G. Colin, C.H. Bayley, J. Pharm. Sci. 54 (1965) 1674–1675.
[19] J.P. Mallari, W.A. Guiguemde, R.K. Guy, Bioorg. Med. Chem. Lett. 19 (2009) 3546–3549.
[20] S.A. Khan, M. Yusuf, Eur. J. Med. Chem. 44 (2009) 2270–2274.
[21] F. Salsi, G. Bulhões Portapilla, K. Schutjajew, Z.A. Carneiro, A. Hagenbach, S. de Albuquerque, P.I. da Silva Maia, U. Abram, J. Fluorine Chem. (2018).
[22] C. Santini, M. Pellei, V. Gandin, M. Porchia, F. Tisato, C. Marzano, Chem. Rev. 114 (2014) 815–862.
[23] F.N. Akladios, S.D. Andrew, C.J. Parkinson, J. Biol. Inorg. Chem. 21 (2016) 931–944.
[24] D. Senthil Raja, N.S. Bhuvanesh, K. Natarajan, Inorg. Chem. 50 (2011) 12852–12866.
[25] E. Ramachandran, D. Senthil Raja, N.S.P. Bhuvanesh, K. Natarajan, Dalton Trans. 41 (2012) 13308–13323.
[26] E. Ramachandran, D.S. Raja, J.L. Mike, T.R. Wagner, M. Zeller, K. Natarajan, RSC Adv. 2 (2012) 8515–8525.
[27] F. Bisceglie, M. Tavone, F. Mussi, S. Azzoni, S. Montalbano, S. Franzoni, P. Tarasconi, A. Buschini, G. Pelosi, J. Inorg. Biochem. 179 (2018) 60–70.
[28] A. Sreekanth, M.R.P. Kurup, Polyhedron 22 (2003) 3321–3332.
[29] B.N. Harikumar, M.R.P. Kurup, T.N. Jayaprakash, Transition Met. Chem. 22 (1997) 507–509.
[30] P. Bindu, M.R.P. Kurup, Transition Met. Chem. 22 (1997) 578–582.
[31] W.J. Geary, Coord. Chem. Rev. 7 (1971) 81–122.
[32] J. Haribabu, K. Jeyalakshmi, Y. Arun, N.S. Bhuvanesh, P.T. Perumal, R. Karvembu, J. Biol. Inorg. Chem. 22 (2017) 461–480.
[33] R. Prabhakaran, R. Karvembu, T. Hashimoto, K. Shimizu, K. Natarajan, Inorg. Chim. Acta 358 (2005) 2093–2096.
[34] N.G. Yernale, M. Bennikallu Hire Mathada, Bioinorg. Chem. Appl. 2014 (2014).
[35] K.M. Raj, B. Vivekanand, G. Nagesh, B. Mruthyunjayaswamy, J. Mol. Struct. 1059 (2014) 280–293.
[36] F.K. Kneubühl, J. Chem. Phys. 33 (1960) 1074–1078.
[37] R. Konakanchi, J. Haribabu, J. Prashanth, V.B. Nishtala, R. Mallela, S. Manchala, D. Gandamalla, R. Karvembu, B.V. Reddy, N.R. Yellu, Appl. Organomet. Chem. 32 (2018) e4415.
[38] D. Kivelson, R. Neiman, J. Chem. Phys. 35 (1961) 149–155.
[39] B. Hathaway, D. Billing, Coord. Chem. Rev. 5 (1970) 143–207.
[40] K.A. Rahman, J. Haribabu, C. Balachandran, N.S. Bhuvanesh, R. Karvembu, A. Sreekanth, Polyhedron 135 (2017) 26–35.
[41] A. Meenongwa, R.F. Brissos, C. Soikum, P. Chaveerach, P. Gamez, Y. Trongpanich, U. Chaveerach, New J. Chem. 39 (2015) 664–675.
[42] L.-D. Wang, K. Zheng, Y.-T. Li, Z.-Y. Wu, C.-W. Yan, J. Mol. Struct. 1037 (2013) 15–22.
[43] M. Ganeshpandian, R. Loganathan, S. Ramakrishnan, A. Riyasdeen, M.A. Akbarsha, M. Palaniandavar, Polyhedron 52 (2013) 924–938.
[44] K. Jeyalakshmi, N. Selvakumaran, N.S. Bhuvanesh, A. Sreekanth, R. Karvembu, RSC Adv. 4 (2014) 17179–17195.
[45] Y.-Q. Li, X.-Y. Li, A.A.F. Shindi, Z.-X. Zou, Q. Liu, L.-R. Lin, N. Li, Synchronous fluorescence spectroscopy and its applications in clinical analysis and food safety evaluation, in: C.D. Geddes (Ed.), Reviews in Fluorescence 2010, Springer New York, New York, NY, 2012, pp. 95–117.
[46] R. Mallela, R. Konakanchi, R. Guda, N. Munirathinam, D. Gandamalla, N.R. Yellu, L.R. Kotha, Inorg. Chim. Acta 469 (2018) 66–75.
[47] T.R. Arun, N. Raman, Spectrochim. Acta Part A Mol. Biomol. Spectrosc. 127 (2014) 292–302.
[48] R. Konakanchi, R. Mallela, R. Guda, L.R. Kotha, Res. Chem. Intermed. 44 (2018) 27–53.
[49] A. Sreekanth, H.-K. Fun, M.P. Kurup, J. Mol. Struct. 737 (2005) 61–67.
[50] N. Karalı, A. Gürsoy, F. Kandemirli, N. Shvets, F.B. Kaynak, S. Özbey, V. Kovalishyn, A. Dimoglo, Bioorg. Med. Chem. 15 (2007) 5888–5904.
[51] F. Kandemirli, T. Arslan, N. Karadayı, E.E. Ebenso, B. Köksoy, J. Mol. Struct. 938 (2009) 89–96.
[52] M. Reichmann, S. Rice, C. Thomas, P. Doty, J. Am. Chem. Soc. 76 (1954) 3047–3053.
[53] J. Marmur, J. Mol. Biol. 3 (1961) 208-IN201.